

Cooperative polymerization of α -helices induced by macromolecular architecture

Ryan Baumgartner¹, Hailin Fu², Ziyuan Song³, Yao Lin^{2*} and Jianjun Cheng^{1,3*}

Catalysis observed in enzymatic processes and protein polymerizations often relies on the use of supramolecular interactions and the organization of functional elements in order to gain control over the spatial and temporal elements of fundamental cellular processes. Harnessing these cooperative interactions to catalyse reactions in synthetic systems, however, remains challenging due to the difficulty in creating structurally controlled macromolecules. Here, we report a polypeptide-based macromolecule with spatially organized α -helices that can catalyse its own formation. The system consists of a linear polymeric scaffold containing a high density of initiating groups from which polypeptides are grown, forming a brush polymer. The folding of polypeptide side chains into α -helices dramatically enhances the polymerization rate due to cooperative interactions of macrodipoles between neighbouring α -helices. The parameters that affect the rate are elucidated by a two-stage kinetic model using principles from nucleation-controlled protein polymerizations; the key difference being the irreversible nature of this polymerization.

The desire to capture the remarkable functionality of biological macromolecules through synthetic analogues has led to the development of a variety of artificial enzymes^{1–3}, molecular motors^{4,5} and machines^{6–8}. These systems are able to carry out basic enzymatic functions such as binding, recognition, and catalysis, as well as more complex functions involving the regulation of molecular assembly^{9–16}. Although artificial systems have advanced in complexity and sophistication, the ability to mimic the spatial and temporal control of natural systems remains limited. In nature, these advanced features are often realized through the implementation of precise structural features and cooperative interactions that accelerate otherwise slow processes^{17,18}. For example, the slow spontaneous polymerization of tubulin is aided by microtubule-organizing centres such as the centrosome¹⁹. Actin polymerization is similarly stimulated by the Arp2/3 complex²⁰. These nucleation factors enable faster polymer growth by lowering the activation energy of nucleation while also regulating the organization of the resulting polymeric arrays^{19,21}. Presently, few systems have adopted a strategy similar to nature where macromolecular or supramolecular structure is used to catalyse and direct the growth of polymers^{16,22}.

Here, we report a polypeptide-based polymerization system whose rate of growth is governed by its macromolecular structure, which is encoded within the polymerization initiator. The system consists of a linear polymeric scaffold containing initiation sites on which amino acid precursors, in the form of *N*-carboxyanhydrides (NCAs), condense to form polypeptide chains. Upon reaching a critical chain length, the polypeptides are able to fold into α -helices. The continued addition of NCA monomers onto the α -helices is found to be catalysed through cooperative dipolar interactions between neighbouring α -helices on the same scaffold. By controlling the structural elements that govern the proximity of growing helices along the scaffold, the extent of this effect on the polymerization can be modulated. The mechanism displayed by this system is a unique example of how the preorganization of structural elements can be used to influence the construction of covalent macromolecules.

Results and discussion

The macroinitiators (PNB_{*n*}), which induce a large rate enhancement of the NCA polymerization, were constructed through the ring-opening metathesis polymerization (ROMP) of trimethylsilyl (TMS) amine substituted *exo*-norbornene (NB) monomers using ruthenium catalyst G3 (Fig. 1a)^{23,24}. The synthesis was relatively straightforward resulting in well-controlled polymers with a low polydispersity index (PDI < 1.1; Supplementary Fig. 1 and Supplementary Table 1). The TMS protected amine groups (NHTMS) positioned along the scaffold serve as initiation sites for the polymerization of NCA monomers, resulting in the subsequent formation of molecular brush polymers. We chose to use the NCA of γ -benzyl-L-glutamate (BLG-NCA) as a model monomer for brush polymer formation due to its straightforward purification and good solubility (Fig. 1a). Additionally, the resulting polymer, poly(γ -benzyl-L-glutamate) (PBLG), has been well studied; it and related polypeptides are known to fold into α -helices upon reaching a length of 8–12 amino acids^{25–27}, corresponding to nearly three helical turns. The polymerization of BLG-NCA monomers initiated by PNB_{*n*} macroinitiators, thus, results in molecular brush polymers containing an array of α -helices spaced along the scaffold. While typically, solvents such as *N,N*-dimethylformamide (DMF) are employed to control the polymerization of NCA monomers by solvating the resulting polypeptides and minimizing electrostatic effects resulting from the macrodipole moments of α -helices, we discovered superior control over the polymerization in chlorinated solvents, such as dichloromethane (DCM), which instead have relatively low dielectric constants (Supplementary Fig. 4 and Supplementary Table 4).

In DCM, the polymerization of BLG-NCA conducted with the macroinitiator PNB₁₀₀ resulted in polypeptide brush polymers with accurate molecular weight (MW) values and low PDI (< 1.05) at initial monomer concentrations ($[M]_0$) as low as 50 mM (Fig. 1b). Despite previous reports of precipitation or turbidity for NCA polymerizations in alternative solvents^{28,29}, the solution remained clear during the entire course of the polymerization.

¹Department of Chemistry, University of Illinois at Urbana-Champaign, Urbana, Illinois 61801, USA. ²Department of Chemistry and Institute of Materials Science, University of Connecticut, Storrs, Connecticut 06269, USA. ³Department of Materials Science and Engineering, University of Illinois at Urbana-Champaign, Urbana, Illinois 61801, USA. *e-mail: jianjunc@illinois.edu; yao.lin@uconn.edu

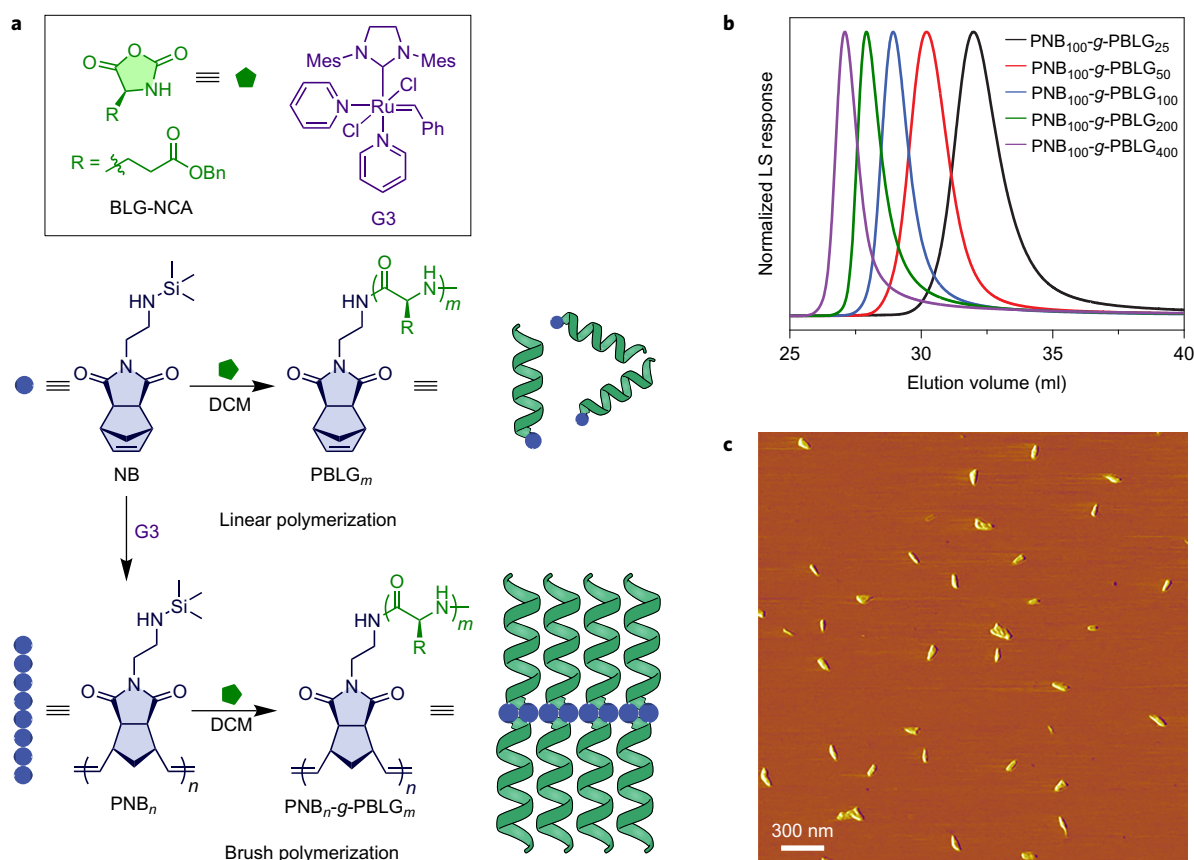


Figure 1 | Synthesis of linear and brush polypeptides. **a**, Polymerization of BLG-NCA initiated by NB forms linear polypeptides (PBLG_m). Ring-opening metathesis polymerization (ROMP) of NB with catalyst G3 forms PNB_n that can act as macroinitiators for the polymerization of BLG-NCA forming brush polymers. The resulting polypeptide chains spontaneously fold into α -helices after obtaining a DP between 8 and 12. The subscripts refer to the average DP. **b**, Light scattering (LS) GPC traces of brush polymers with varying side chain lengths initiated by PNB₁₀₀ demonstrating excellent control over the polymerization. **c**, AFM phase image of PNB₄₀₀-g-PBLG₅₀ polymers imaged in tapping mode on freshly cleaved mica revealing rigid rod-like structure of brush polymers.

High conversions of monomer resulted (98%) even at a degree of polymerization (DP) of 400, which is particularly noteworthy compared to the analogous linear polymerization initiated by NB that only obtained a conversion of 32% at a designed DP of 200 after 24 h. This unusual difference, however, enabled us to synthesize some of the highest MW synthetic polypeptide materials known to date ($M_n = 4.3 \times 10^7$ Da, PDI = 1.07) in a convenient one-pot reaction (Supplementary Fig. 5 and Supplementary Table 6). Visualization using atomic force microscopy (AFM) confirmed the low PDI and rod-like structure of these large unimolecular macromolecules (Fig. 1c; Supplementary Figs 9–11).

The most remarkable feature of the polymerization of BLG-NCA initiated by PNB_n-based macroinitiators, however, was the exceptionally large polymerization rate compared with the analogous linear polymerization initiated by NB. For example, under identical conditions (DCM, $[M]_0 = 50$ mM, initial NHTMS concentration $[I]_0 = 0.25$ mM) the brush polymerization initiated by PNB₁₀₀ completed in just under 1 h, while the linear polymerization initiated by NB was not complete within 24 h (Fig. 2a). This marked difference in rate is astonishing bearing in mind that the initiators for both linear and brush polymerizations are nearly identical, chemically, and differ only in the connectivity and proximity of initiating groups. Interestingly, this striking rate difference is not observed in traditionally used solvents such as DMF²³. Although NCA polymerizations are widely known to be plagued by other more rapid propagation mechanisms involving deprotonation of the N–H bond and subsequent polymerization of the activated monomer^{30–32}, the absence of linear polymer that would result from monomer

mediated initiation suggests the absence of this propagation mechanism, in line with previous reports of TMS mediated polymerization of NCAs^{24,33}.

In order to elucidate factors leading to this substantial rate enhancement in DCM, we utilized *in situ* Fourier transform infrared spectroscopy (FTIR) to monitor the progress of the NCA polymerization in more detail. We observed that, as with the linear polymerization (Supplementary Fig. 21)³⁴, the consumption of monomer proceeded in two distinct stages (Fig. 2b). During the first stage, the disappearance of NCA monomer ($1,865$ cm⁻¹, $1,793$ cm⁻¹) is relatively slow, and the resulting polypeptides take on the form of solvated coils evidenced by the increase in absorbance at $1,658$ cm⁻¹ (ref. 35). This primary nucleation stage is followed by a sudden transition to a second, faster elongation stage that is characterized by a rapid depletion of NCA monomer. During this stage, the amide I and II regions show increasing absorbance at $1,655$ cm⁻¹ and $1,549$ cm⁻¹, respectively, which is typical of α -helical secondary structures³⁵. Monitoring changes in circular dichroism (CD) during the polymerization also confirms the clear formation of right-handed α -helical structures at the onset of the second stage (Fig. 2c). The critical length of the side-chains at the transition point determined from kinetic models (*vide infra*) ranges from 8–12, in excellent agreement with the length at which α -helices become stable^{25–27}. This data suggests that in addition to the rate differences determined by the structure of the initiator, the folding of the polypeptides into α -helices also induces a more favourable polymerization process.

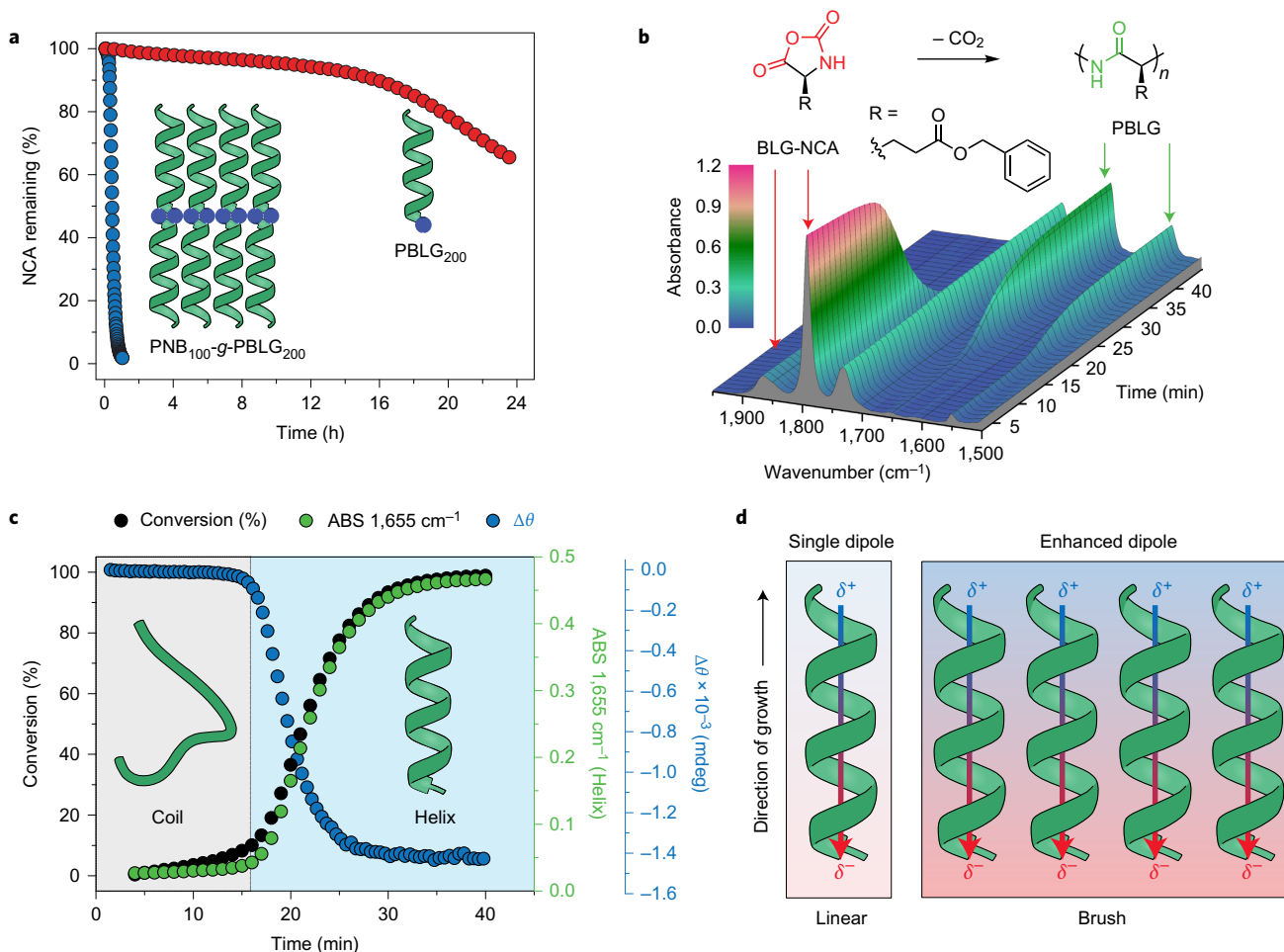


Figure 2 | Rate difference and kinetic pattern of NCA polymerization. **a**, Conversion of BLG-NCA in DCM using NB (red) or PNB₁₀₀ (blue) as initiators revealing marked rate enhancement using PNB₁₀₀. $[M]_0 = 50$ mM; $[I]_0 = 0.25$ mM. The subscripts refer to the average DP. **b**, Polymerization of BLG-NCA initiated by PNB₁₀₀. Changes in the concentration of BLG-NCA and product are shown by changes in the FTIR spectrum over the duration of the polymerization. Absorbance at 1,733 cm^{-1} refers to the benzyl ester. **c**, Comparison between the conversion of BLG-NCA (black) at 1,793 cm^{-1} , the increase in absorbance corresponding to the formation of α -helix (green) at 1,655 cm^{-1} , and the change in ellipticity (blue) as monitored by CD at a wavelength of 227.9 nm. The conversion of monomer in the early stages of the polymerization proceeds without the onset of secondary structure. Only when the α -helix appears does the polymerization rate increase dramatically. **d**, Representation of the macrodipole of a growing α -helix. The positive pole is located at the actively growing N-terminus. In the brush system, the macroinitiator constrains the helices in an approximately parallel array where the dipoles of neighbouring α -helices enhance one another, leading to a faster rate of growth in the brush system.

These two factors, however, appear to be related. Consider the values of the rate constants for the primary nucleation stage (k_1) and the second elongation phase (k_2) for both the linear and brush systems. While the semilogarithmic plots reveal pseudo-first order kinetics during both stages of the polymerization (Supplementary Fig. 15), the rate constants cannot be accurately determined from these plots due to the uncertainty in the number of actively growing chains. Nonetheless, the kinetic models developed for the polymerization (*vide infra*) reveal a >1,000-fold increase in the magnitude of the rate constant for the brush system (k_2/k_1), upon formation of α -helices. Meanwhile, the formation of α -helices in the linear polymerization only increases the rate of polymerization by less than a factor of 10 (Supplementary Table 8). This marked difference is largely due to increases in the magnitude of k_2 , which is over 1,000 times larger in the brush polymerization system. The value of k_1 between the linear and brush systems differs by only a factor of 10, being larger in the brush system. The differences in absolute rate between the linear and brush systems are, in fact, so profound that the brush polymerization initiated by PNB₁₀₀ can be carried out in the presence of NB without the formation of any linear polymer (Supplementary Fig. 13). The

data extracted from the values of the rate constants suggests that PBLG helices grown in proximity along the PNB scaffold during the second stage benefit from greater rate enhancement than random coils grown along the scaffold in the primary phase.

If we consider the linear and brush polypeptide systems, the key difference stems from the proximity and orientation of the resulting polypeptide chains, which are governed in turn by the structure of the initiator. In the brush polymer system, the NHTMS-based initiating groups are constricted in proximity along the polymer backbone through covalent bonds. As a consequence, the resulting polypeptide chains are forced to grow outwards from the scaffold, additionally constricting the direction of growth along the brush scaffold. Furthermore, this proximity-induced catalysis is only observed for the brush system in chlorinated solvents of low dielectric constant. These results can be understood by taking into account the macrodipoles of the α -helices. Within an individual α -helix, the hydrogen bonding network results in a large dipole moment along the helical axis with the negative pole located at the C-terminus, and the positive pole located at the active polymerization centre situated at the N-terminus. We reason that this macrodipole is the cause for not only the transition from k_1 to k_2 ,

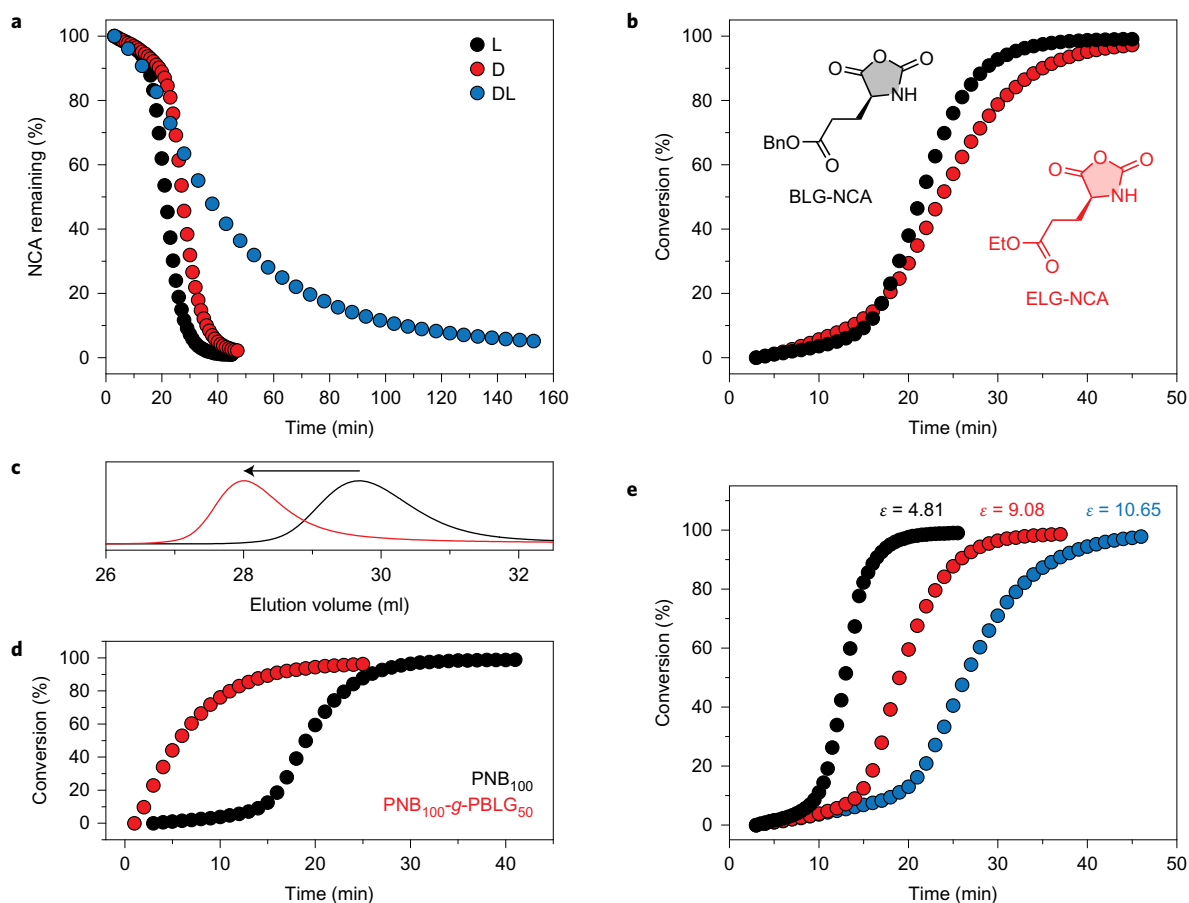


Figure 3 | Kinetic studies of brush polymerization. **a**, Polymerization of L (BLG-NCA), D (BDG-NCA), and DL (BDLG-NCA) isomers of γ -benzyl-glutamate NCA initiated by PNB_{100} . Although both the L and D monomer transition into an α -helix, the DL monomer propagates as a random coil for the entire duration of the polymerization resulting in the lack of a second stage. **b**, Conversion of BLG-NCA (black) and ELG-NCA (red) over time demonstrating identical rates. **c**, Normalized GPC-LS traces of PNB_{100} - g - PBLG_{50} before (black) and after (red) the addition of an additional 50 equiv. of BLG-NCA to the reaction solution revealing complete addition of monomer to growing polymer chains. **d**, Kinetics of BLG-NCA polymerization initiated by PNB_{100} (black) or PNB_{100} - g - PBLG_{50} (red). The lack of primary nucleation stage for PNB_{100} - g - PBLG_{50} suggests continuation of the helical propagation stage. **e**, Relationship between polymerization rate and dielectric constant. Polymerization kinetics of BLG-NCA are shown in chloroform (black), DCM (red), and 1,2-dichloroethane (blue). All polymerizations were performed in DCM with NCA at a concentration of 50 mM and PNB_{100} at a concentration of 1.0 mM unless otherwise specified.

but also for the enhanced propagation rates of the brush system over the linear polymerization. Within a single polypeptide chain, for example, the conformational transition from coil to helix and concomitant formation of a macrodipole moment will greatly change the electrostatic environment at the growing chain end. When favourable, this environment will lead to an increased rate of polymerization (k_2) since this environment is tethered to the propagating chain end. When this effect is translated to the brush polymerization system, which contains an approximately parallel array of α -helices, a large electric field results, further strengthening the electrostatic environment at the chain ends resulting in further enhancement of k_2 (Fig. 2d). While mechanistic details are under further investigation, the terminal amide N-H bonds, which carry the positive dipole, appear to be positioned ideally for binding to the oxygen of the 5-carbonyl of the incoming NCA, which is expected to lower the activation energy for the formation of the tetrahedral intermediate after nucleophilic attack of the amine (the rate limiting step of the polymerization)^{36–38}. Our proposed mechanism appears to bear an interesting resemblance to the Juliá-Colonna epoxidation of chalcone which also involves binding of substrate to the amide groups of an α -helix N-terminus^{39,40}. Furthermore, electrostatically induced catalysis has been reported on reactions of small molecules via the use of external electric

fields⁴¹, however, this macromolecular system provides an opportunity to examine how these effects can be implemented using the tertiary structure of macromolecules.

To further test our assertion, we sought to perturb several important elements required for this polymerization phenomenon. The most important element we aimed to eliminate or diminish was the macrodipole of the α -helix. The macrodipole is carried along the backbone hydrogen bonding network and it follows that breaking this network should reduce the polymerization rate since individual amide dipoles within an unstructured random chain do not couple as efficiently. In addition, breaking the architecture of the α -helix destroys the organized configuration at the growing chain end. Strong helix breaking solvents such as dichloroacetic acid or trifluoroacetic acid are not compatible with the polymerization itself, however, polymerization of the racemic DL monomer prevents formation of the α -helix. While the D and L monomers of γ -benzyl-glutamate NCA individually show comparable polymerization rates, a 1:1 mixture of the two monomers resulted in a diminished rate of polymerization and the disappearance of the two-stage propagation pattern, instead resulting in an apparent first order decay (Fig. 3a). The single propagation rate of the DL monomer is due to the lack of any change in secondary structure, instead propagating as a random coil for the entire duration of the polymerization. The

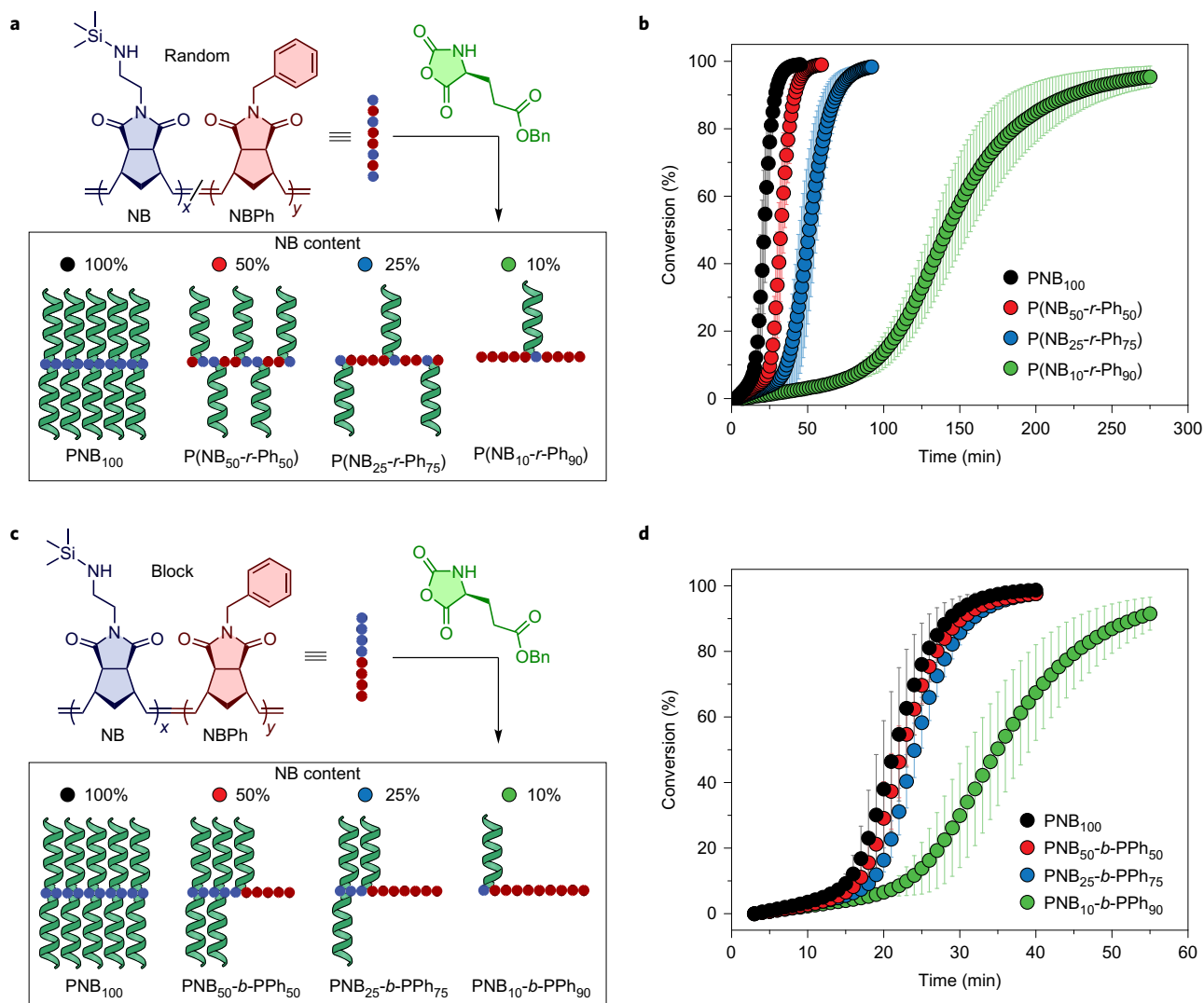


Figure 4 | Kinetic studies of random and block macroinitiators. **a**, Random copolymer scaffolds composed of NB and Ph and the resulting brush polymers. Copolymers with decreasing NB content result in scaffolds with increasing average distance between initiation sites. **b**, Conversion of BLG-NCA over time initiated from random copolymers $P(\text{NB}_x\text{-}r\text{-Ph}_y)$ showing a decrease in polymerization rate with increasing interhelical distance. The subscripts refer to the average DP. **c**, Block copolymer scaffolds composed of NB and Ph and the resulting brush polymers. For these polymers, a decrease in NB content does not result in a change in distance between initiators. **d**, Conversion of BLG-NCA over time initiated from block copolymers $\text{PNB}_x\text{-}b\text{-PPh}_y$ revealing identical rates for NB block sizes of 25, 50 and 100. The decreased rate of $\text{PNB}_{10}\text{-}b\text{-PPh}_{90}$ results from a low number of resulting helices. The subscripts refer to the average DP. All polymerizations were conducted in DCM at $[\text{M}]_0 = 50 \text{ mM}$ and $[\text{I}]_0 = 1.0 \text{ mM}$. Error bars represent standard deviations from three independent measurements.

decreased propagation rate, however, is likely due to both changes in the secondary and tertiary structure of the polypeptide. As indicated before, the decreased dipole moment of the random coil polypeptide results in a diminished polymerization rate for a single isolated polypeptide chain. When the effects of the tertiary (or macromolecular) structure of the brush are considered, where polymer chains are in close proximity, the decreased dipole of the random coils results in a reduced interchain interaction strength between neighbouring polypeptides compared to the α -helical brush system. This latter effect is more clearly demonstrated when considering the faster propagation rate exhibited by the brush polymerization of the DL monomer over the linear polymerization of the L monomer.

Other important elements of the polymerization were also assessed. For instance, additional NCA monomers of high purity whose products form α -helices, such as γ -ethyl-L-glutamate NCA (ELG-NCA), showed two propagation rates and retained the enhanced polymerization rate in the brush system (Fig. 3b). Ethylene glycol substituted L-lysine NCA ($\text{EG}_2\text{-Lys-NCA}$)⁴²,

which is more difficult to purify, also had enhanced propagation rates over the linear counterparts, albeit, both rates were slightly slower (Supplementary Fig. 21). Additionally, when the polymerization was initiated with $\text{PNB}_{100}\text{-}g\text{-PBLG}_{50}$, we observed complete addition of BLG-NCA to the pre-existing brush polymer, which maintained a low PDI and accurate MW (Fig. 3c). The consumption of monomer proceeded immediately, devoid of the slow nucleation stage ruling out a mechanism of the general autocatalytic type and supporting a mechanism consisting of one nucleation phase (Fig. 3d and Supplementary Fig. 23). The polymerization was also sensitive to changes in the dielectric constant of the media, which is anticipated for electrostatic involvement. Carrying out the polymerization in various chlorinated solvents, we found that in those having a lower dielectric constant, such as chloroform ($\epsilon = 4.81$), the polymerization was most rapid, whereas in 1,2-dichloroethane ($\epsilon = 10.56$) the polymerization was slowest (Fig. 3e). When methylcyclohexane ($\epsilon = 2.02$) was added to the polymerization, further rate enhancement was observed (Supplementary Fig. 22).

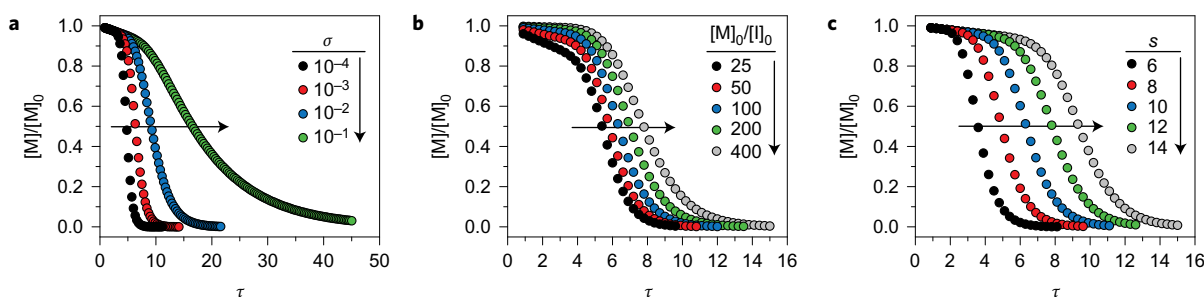
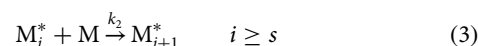
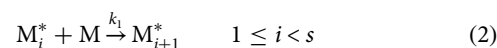


Figure 5 | Simulations with cooperative covalent polymerization model. a–c, Plots of the fraction of monomer versus rescaled time ($\tau = tk_1[M]_0$) for test cases with $s = 10$, $[M]_0/[I]_0 = 100$ at selected values of σ (**a**), $s = 10$, $\sigma = 10^{-3}$, at selected values of $[M]_0/[I]_0$ (**b**), and $[M]_0/[I]_0 = 100$, $\sigma = 10^{-3}$, at selected values of s (**c**). Fraction of monomer was calculated using the numerical solutions of equations (4) to (8).

The control over the brush polymer scaffold provided by ROMP allowed us to further probe the effect of polymer chain proximity on the polymerization kinetics. We investigated this by synthesizing several new polymeric scaffolds of varying composition and connectivity. Random copolymers of NB with inactive spacer groups containing a phenyl moiety (Ph), for instance, were synthesized which allowed us to access brush polymers with a lower grafting density of α -helices (Fig. 4a; see also Supplementary Fig. 2 and Supplementary Table 2). By changing the feeding ratio between the two monomers forming $P(\text{NB}_x\text{-}r\text{-Ph}_y)$ random copolymers, the average distance between initiation sites along the scaffold could be tuned, allowing us to assess the effects of interhelical distance on the polymerization rate. Using ozonolysis to cleave the PBLG chains from the backbone, the decrease in grafting density of the copolymers with decreasing NB content was verified (see Supplementary Information for further details). When the polymerization of BLG-NCA was carried out with the $P(\text{NB}_{50}\text{-}r\text{-Ph}_{50})$ random copolymer scaffold which possess a lower density of initiating groups, we again observed a two-stage polymerization, however, the polymerization activity was diminished compared to the polymerization carried out with PNB_{100} (Fig. 4b). The continued substitution of NB units for Ph units along the scaffold, forming $P(\text{NB}_{25}\text{-}r\text{-Ph}_{75})$ and $P(\text{NB}_{10}\text{-}r\text{-Ph}_{90})$ copolymers, had the effect of decreasing the polymerization rate even further. This revealed that at identical overall concentrations of initiating NB groups, the scaffolds containing higher amounts of NB possessed a faster polymerization rate. That is to say that α -helices grown closer together polymerized faster than those more isolated relative to one another. In order to rule out concomitant changes of macromolecular size with changes in α -helical grafting density, several control experiments were conducted with copolymer scaffolds having longer backbones (PNB_{200}). The resulting macromolecules of precisely twice the MW but identical grafting density showed polymerization activity that was indistinguishable from the shorter scaffolds, suggesting that macromolecular size does not play a significant role in the polymerization (Supplementary Fig. 20). Interestingly, the connectivity of the NB and Ph monomers of the scaffold can be synthetically rearranged into block domains forming $\text{PNB}_x\text{-}b\text{-PPh}_y$ block copolymers (Fig. 4c; see also Supplementary Fig. 3 and Supplementary Table 3). These scaffolds, which contain an identical number of α -helices as the random copolymer scaffolds, differ only in that the α -helices have been artificially placed in close proximity to one another. For $\text{PNB}_x\text{-}b\text{-PPh}_y$ scaffolds containing block domains of 25 NB units or greater, we observe polymerization activity that is identical to that exhibited by the PNB_{100} polymer scaffold (Fig. 4d). The $\text{PNB}_{10}\text{-}b\text{-PPh}_{90}$ block copolymer, however, possessed a slightly decreased polymerization rate in comparison to the block copolymer scaffolds with higher NB content. This is expected since a limit will eventually be reached in which the continued decline in the block size of NB monomers results in α -helices

that remain close in proximity, but few in number such that the cooperative interactions begin to diminish. The extreme of this case resembles the linear polymer system, where dipole coupling is weakest. Compared to the $P(\text{NB}_{10}\text{-}r\text{-Ph}_{90})$ random copolymer scaffolds, however, the block $\text{PNB}_{10}\text{-}b\text{-PPh}_{90}$ copolymer scaffolds of the same NB composition exhibit significantly greater polymerization rates (Fig. 4b,d). These observations confirm the essential role of helical proximity in the rate enhancement of this polymerization.

The dependence of side-chain propagation rate on the brush grafting density reveals an intriguing cooperative behaviour facilitated by neighbouring helical polypeptides within the same macromolecule (that is, an effect of tertiary structure). Indeed, this effect is rather unique compared to other brush polymer systems that show a similar or often decreased rate of polymerization compared to the respective linear analogues^{43,44}. While never before described in irreversible covalent polymerization, this cooperative growth mechanism is well studied and widespread in supramolecular polymerization, where proteins or synthetic monomer units are instead brought together through reversible and non-covalent interactions to form one-dimensional polymeric arrays. For example, Oosawa¹⁸ proposed a cooperative supramolecular growth mechanism for actin polymerization that consists of two phases: first, the monomers slowly segregate into a linear chain, which, upon reaching a critical length (the nucleus) the linear chain can rearrange into a helix. At this stage, chain growth becomes more favourable due to additional secondary interactions between the incoming monomer and the polymer chain. Herein, we adapt this cooperative growth mechanism to analyse the polymerization of helical polypeptides in the brush polymers, by treating the addition of monomer instead as an irreversible process. Consider the simplest model possible for this cooperative covalent polymerization under which the only allowed reactions are initiation (equation (1)) and the stepwise addition of monomer, $[M]$, onto the active chains ((equations (2) and (3)). There exists a unique chain length, s , after which the propagation constant changes due to folding of the coil into an α -helix. We denote an active polymer of degree of polymerization i by M_i^* , and its concentration by $[M_i^*]$, where $*$ represents the reactive end. The initial concentration of monomer and initiator are represented by $[M]_0$ and $[I]_0$, respectively. The kinetic constants for initiation (k_i) and the two successive growth stages (k_1 and k_2) are then defined by:



For clarity, the production of CO_2 is ignored in the reaction scheme. Spectroscopic studies on the brush polymerization as well as other

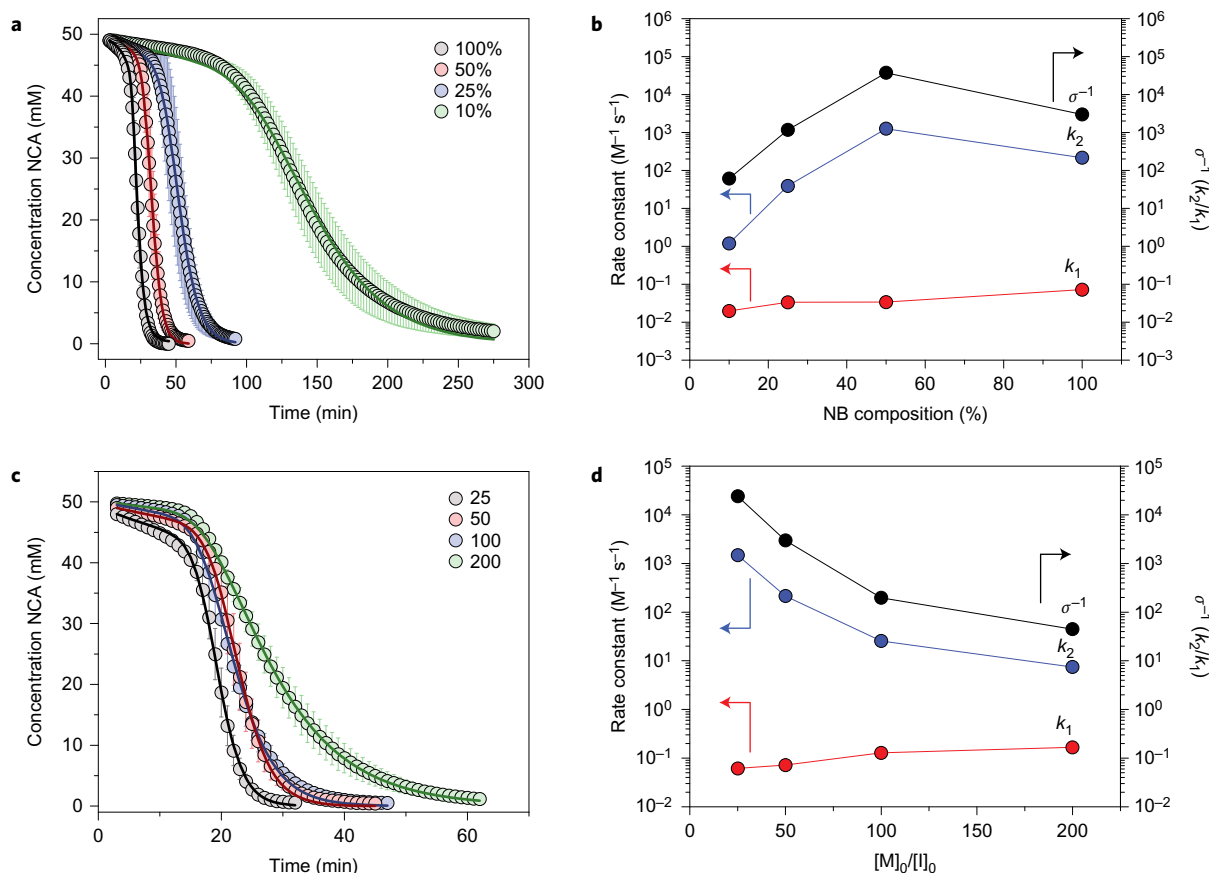


Figure 6 | Analysis of brush polymerization with two-stage kinetic model. **a**, Kinetic data (circles) obtained from the polymerization of BLG-NCA with $\text{PNB}_{x-r}\text{-PPh}_y$ random copolymer macroinitiators of varying NB content (mol%) is fit with the two-stage kinetic model (solid lines) at $s=10$, $[\text{M}]_0 = 50$ mM, and $[\text{I}]_0 = 1.0$ mM. **b**, Extracted rate constants for the primary nucleation stage (k_1) and the second elongation stage (k_2) from **a**, and calculated σ^{-1} all support a higher cooperativity for higher helix grafting density. The changes in cooperativity largely arise from changes in k_2 , the rate of helical propagation. **c**, Kinetic data (circles) obtained from the polymerization of BLG-NCA with PNB_{100} at varying $[\text{M}]_0/[\text{I}]_0$ ratios is fit with the two-stage kinetic model (solid lines) at $s=10$ and $[\text{M}]_0 = 50$ mM. **d**, Extracted rate constants for the primary nucleation stage (k_1) and the second elongation stage (k_2) from **c**, and calculated σ^{-1} . The results show a decrease in cooperativity with increasing DP, possibly due to the additional conformational freedom of longer chains. Changes in cooperativity are largely due to changes in k_2 . Error bars represent standard deviations from three independent measurements.

NCA polymerizations reveal a fast initiation event relative to propagation ($k_i \gg k_1$) and we accordingly assume $[\text{M}_i^*] = [\text{I}]_0$, $[\text{M}] = [\text{M}]_0 - [\text{I}]_0$, at the time of the first data point ($t = 3$ min). It is straightforward, then, to write the kinetic equations corresponding to the scheme above, and find numerical solutions to them:

$$\frac{\partial[\text{M}]}{\partial t} = -k_1[\text{M}] \sum_{i=1}^{s-1} [\text{M}_i^*] - k_2[\text{M}] \sum_{i=s}^{\infty} [\text{M}_i^*] \quad (4)$$

$$\frac{\partial[\text{M}_i^*]}{\partial t} = -k_1[\text{M}][\text{M}_i^*] \quad i = 1 \quad (5)$$

$$\frac{\partial[\text{M}_i^*]}{\partial t} = k_1[\text{M}]([\text{M}_{i-1}^*] - [\text{M}_i^*]) \quad 1 < i < s \quad (6)$$

$$\frac{\partial[\text{M}_i^*]}{\partial t} = k_1[\text{M}][\text{M}_{i-1}^*] - k_2[\text{M}][\text{M}_i^*] \quad i = s \quad (7)$$

$$\frac{\partial[\text{M}_i^*]}{\partial t} = k_2[\text{M}]([\text{M}_{i-1}^*] - [\text{M}_i^*]) \quad i > s \quad (8)$$

In analogy to the cooperativity factor in supramolecular polymerization, we can define the dimensionless ratio $\sigma = k_1/k_2$ where a small value of σ ($\ll 1$) implies a highly cooperative reaction, and $\sigma = 1$ implies no cooperativity. The cooperative covalent polymerization

is thus intrinsically controlled by two dimensionless parameters, the critical chain length, s , and the cooperativity, σ . Transformation of equations (4) to (8) into dimensionless parameters more clearly shows this relationship (see Supplementary equations (1) to (6)). Solving the differential equations numerically for different s , σ , and initial monomer-to-initiator ratios ($[\text{M}]_0/[\text{I}]_0$) yields the various kinetic curves shown in Fig. 5a–c, where the fraction of remaining monomer is plotted against dimensionless time $\tau = tk_1M_0$. The model is able to correctly account for and describe the course of monomer consumption over time as observed in the experimental data, and the shape of the curve is heavily influenced by s , σ , and $[\text{M}]_0/[\text{I}]_0$ ratio, as expected.

This cooperative covalent model was then applied to the data generated from the random copolymer scaffolds that showed a wide range of rates and cooperativity due to variation of the helical distances. The optimized fits for this data shown in Fig. 6a demonstrate that the model is able to describe the data from the experiments in excellent agreement. The critical chain length s was determined to be 10 ± 2 for all four samples, again, in agreement with the predicted length at which α -helices become stable. The rate constant, k_1 , for the four reactions did not appear to vary significantly (Fig. 6b), increasing only slightly with increasing grafting density. This indicates that prior to the formation of α -helices, the coupling of amide dipoles contained within short, coil-like polypeptides has limited impact on the reaction. In contrast, the

density of helices strongly affects k_2 . Comparing P(NB_{10-r}-Ph₉₀) and P(NB_{50-r}-Ph₅₀) random copolymers, for example, reveals rate constants that increase over three orders of magnitude from 1.2 M⁻¹ s⁻¹ to 1.26 × 10³ M⁻¹ s⁻¹, respectively. The result shows that a strong cooperative behaviour can be induced upon the formation of helical macrodipoles in the proximity to the active polymerization site. The model was further tested by changing the [M]₀/[I]₀ feeding ratios, keeping the NB content of the backbone fixed at 100%. With [M]₀ constant at 50 mM, [I]₀ was systematically decreased resulting in the kinetic traces shown in Fig. 6c. As expected, s obtained from the model fitting remained at 10 ± 2 for the four conditions. The rate constant k_1 increased only slightly at higher [M]₀/[I]₀ ratios, while k_2 , interestingly, decreased (Fig. 6d). While inhibitory effects from generated CO₂ are possible for this observation and cannot be ruled out conclusively, the diminishing rate constant may instead suggest attenuation of the effect of the macrodipole when the helical chains grow longer and obtain greater conformational freedom. Thus, a more sophisticated model should take into account the possible variation of microscopic rate constants in the second stage of propagation, which is the subject of our future studies.

The system presented here is a remarkable example of a polymerization whose rate is governed by the three-dimensional structure of the resulting polymer, which is in turn dictated by the structure of the initiator. The present system is able to generally mimic the key features of centromeres, albeit, by a unique mechanism in which the cooperative electrostatic interactions between growing helices enhance the rate of polymerization. We expect interactions of this kind to contribute to future developments in polymer and supramolecular chemistry, as well as to our understanding of the cytoskeleton, protein function, and catalysis.

Methods

Full experimental details and characterization of compounds can be found in the Supplementary Information.

Backbone synthesis (ROMP polymerizations). In a glovebox, NB (4 mg, 0.014 mmol) was dissolved in dry DCM in a silanized vial, then G3 catalyst (1 mg ml⁻¹ in DCM) was added at the desired [M]/[I] ratio, such that the final concentration of NB was 0.02 M. The reaction was stirred at 23 °C for 20 min per each 100 repeating units in the final polymer. The polymerization was terminated with 4 μl ethyl vinyl ether. An identical procedure was followed for random copolymers (PNB_{x-r}-PPh_y) utilizing the proper monomer ratios. Block copolymers (PNB_x-b-PPh_y) were synthesized by first polymerizing the desired block length of Ph in DCM (0.04 M < [Ph] < 0.1 M) with the proper amount of G3 solution. After completion of the first block, the desired amount of NB in DCM (10 mg ml⁻¹) was added such that [Ph] + [NB] = 0.02 M. The polymerization was allowed to run until completion (approx. 10 min), then quenched with ethyl vinyl ether (1 μl mg⁻¹ of polymer). All initiator solutions were stored in the glovebox and used directly for NCA polymerizations.

Typical NCA polymerization. In a glovebox, BLG-NCA (5 mg, 0.019 mmol) was weighed into a silanized vial and dissolved in DCM. A proper volume of initiator (~0.02 M in DCM) was added at the desired [M]/[I] ratio such that the final concentration of monomer was 0.05 M. For *in situ* kinetic analysis, the solution was transferred into a 0.1 mm amalgamated KBr liquid transmission cell, removed from the glovebox, and placed into the FTIR instrument. For analysis of resulting unfractionated polymers, polymerization solutions were analyzed by drying *in vacuo* and dissolving in DMF containing 0.1 M LiBr for GPC analysis.

Kinetic modelling. Experimental data was fit to the two-stage polymerization model by iteratively solving the differential equations at a given set of initial polymerization conditions ([M]₀ and [I]₀) for various k_1 , k_2 and s . The parameters that returned the minimum sum of squares of the residuals were selected.

Data availability. All the data generated and/or analysed during the current study are available from the corresponding authors on reasonable request.

Received 24 May 2016; accepted 2 December 2016;
published online 6 February 2017

References

- Breslow, R. Biomimetic chemistry and artificial enzymes: catalysis by design. *Acc. Chem. Res.* **28**, 146–153 (1995).
- Dong, Z., Luo, Q. & Liu, J. Artificial enzymes based on supramolecular scaffolds. *Chem. Soc. Rev.* **41**, 7890–7908 (2012).
- Kuah, E., Toh, S., Yee, J., Ma, Q. & Gao, Z. Enzyme mimics: advances and applications. *Chem. Eur. J.* **22**, 8404–8430 (2016).
- Lund, K. *et al.* Molecular robots guided by prescriptive landscapes. *Nature* **465**, 206–210 (2010).
- Wickham, S. F. J. *et al.* A DNA-based molecular motor that can navigate a network of tracks. *Nat. Nanotechnol.* **7**, 169–173 (2012).
- Erbas-Cakmak, S., Leigh, D. A., McTernan, C. T. & Nussbaumer, A. L. Artificial molecular machines. *Chem. Rev.* **115**, 10081–10206 (2015).
- Browne, W. R. & Feringa, B. L. Making molecular machines work. *Nat. Nanotechnol.* **1**, 25–35 (2006).
- van Dongen, S. F. M., Cantekin, S., Elemans, J. A. A. W., Rowan, A. E. & Nolte, R. J. M. Functional interlocked systems. *Chem. Soc. Rev.* **43**, 99–122 (2014).
- Epstein, I. R. & Xu, B. Reaction-diffusion processes at the nano- and microscales. *Nat. Nanotechnol.* **11**, 312–319 (2016).
- Boekhoven, J., Hendriksen, W. E., Koper, G. J. M., Eelkema, R. & van Esch, J. H. Transient assembly of active materials fueled by a chemical reaction. *Science* **349**, 1075–1079 (2015).
- Sadownik, J. W., Mattia, E., Nowak, P. & Otto, S. Diversification of self-replicating molecules. *Nat. Chem.* **8**, 264–269 (2016).
- Lewandowski, B. *et al.* Sequence-specific peptide synthesis by an artificial small-molecule machine. *Science* **339**, 189–193 (2013).
- Korevaar, P. A. *et al.* Pathway complexity in supramolecular polymerization. *Nature* **481**, 492–496 (2012).
- Aliprandi, A., Mauro, M. & De Cola, L. Controlling and imaging biomimetic self-assembly. *Nat. Chem.* **8**, 10–15 (2016).
- Korevaar, P. A., Newcomb, C. J., Meijer, E. W. & Stupp, S. I. Pathway selection in peptide amphiphile assembly. *J. Am. Chem. Soc.* **136**, 8540–8543 (2014).
- Yu, Z. *et al.* Simultaneous covalent and noncovalent hybrid polymerizations. *Science* **351**, 497–502 (2016).
- Zhao, D. & Moore, J. S. Nucleation-elongation: a mechanism for cooperative supramolecular polymerization. *Org. Biomol. Chem.* **1**, 3471–3491 (2003).
- Oosawa, F. & Asakura, S. *Thermodynamics of the Polymerization of Protein* (Academic Press, 1975).
- Luders, J. & Stearns, T. Microtubule-organizing centres: a re-evaluation. *Nat. Rev. Mol. Cell Biol.* **8**, 161–167 (2007).
- Dominguez, R. & Holmes, K. C. Actin structure and function. *Annu. Rev. Biophys.* **40**, 169–186 (2011).
- De Greef, T. F. A. *et al.* Supramolecular polymerization. *Chem. Rev.* **109**, 5687–5754 (2009).
- McHale, R., Patterson, J. P., Zetterlund, P. B. & O'Reilly, R. K. Biomimetic radical polymerization via cooperative assembly of segregating templates. *Nat. Chem.* **4**, 491–497 (2012).
- Lu, H., Wang, J., Lin, Y. & Cheng, J. One-pot synthesis of brush-like polymers via integrated ring-opening metathesis polymerization and polymerization of amino acid *N*-carboxyanhydrides. *J. Am. Chem. Soc.* **131**, 13582–13583 (2009).
- Lu, H. & Cheng, J. *N*-Trimethylsilyl amines for controlled ring-opening polymerization of amino acid *N*-carboxyanhydrides and facile end group functionalization of polypeptides. *J. Am. Chem. Soc.* **130**, 12562–12563 (2008).
- Goodman, M., Verdini, A. S., Toniolo, C., Phillips, W. D. & Bovey, F. A. Sensitive criteria for the critical size for helix formation in oligopeptides. *Proc. Natl Acad. Sci. USA* **64**, 444–450 (1969).
- Rinaudo, M. & Domard, A. Circular dichroism studies on α -L-glutamic acid oligomers in solution. *J. Am. Chem. Soc.* **98**, 6360–6364 (1976).
- Mutter, M. The influence of the macromolecular protecting group in conformational studies on polyoxyethylene-bound peptides. *Macromolecules* **10**, 1413–1414 (1977).
- Ballard, D. G. H. & Bamford, C. H. The heterogeneous polymerization of α -*N*-carboxyamino-acid anhydrides. *J. Chem. Soc.* 1039–1044 (1959).
- Komoto, T., Akaishi, T., Oya, M. & Kawai, T. Crystallization of polypeptides in the course of polymerization. I: Growth mechanism of poly-L- and DL-alanine crystals. *Makromol. Chem.* **154**, 151–159 (1972).
- Hadjichristidis, N., Iatrou, H., Pitsikalis, M. & Sakellariou, G. Synthesis of well-defined polypeptide-based materials via the ring-opening polymerization of α -amino acid *N*-carboxyanhydrides. *Chem. Rev.* **109**, 5528–5578 (2009).
- Deming, T. J. *Polypeptide and Polypeptide Hybrid Copolymer Synthesis via NCA Polymerization* (Springer, 2006).
- Blout, E. R. & Idelson, M. Polypeptides IX. the kinetics of strong-base initiated polymerizations of amino acid-*N*-carboxyanhydrides. *J. Am. Chem. Soc.* **78**, 3857–3858 (1956).
- Lu, H. & Cheng, J. Hexamethyldisilazane-mediated controlled polymerization of α -amino acid *N*-carboxyanhydrides. *J. Am. Chem. Soc.* **129**, 14114–14115 (2007).
- Lundberg, R. D. & Doty, P. Polypeptides XVII. a study of the kinetics of the primary amine-initiated polymerization of *N*-carboxyanhydrides with special reference to configurational and stereochemical effects. *J. Am. Chem. Soc.* **79**, 3961–3972 (1957).

35. Blout, E. R. & Asadourian, A. Polypeptides. V. the infrared spectra of polypeptides derived from γ -benzyl-L-glutamate. *J. Am. Chem. Soc.* **78**, 955–961 (1956).
36. Ling, J. & Huang, Y. Understanding the ring-opening reaction of α -amino acid N-carboxyanhydride in an amine-mediated living polymerization: a DFT study. *Macromol. Chem. Phys.* **211**, 1708–1711 (2010).
37. Kricheldorf, H. R. *α -Aminoacid-N-Carboxy-Anhydrides and Related Heterocycles* (Springer, 1987).
38. Weingarten, H. Kinetics and mechanisms of the polymerization of N-carboxy- α -amino acid anhydrides. *J. Am. Chem. Soc.* **80**, 352–355 (1958).
39. Kelly, D. R. & Roberts, S. M. The mechanism of polylysine catalysed asymmetric epoxidation. *Chem. Commun.* 2018–2020 (2004).
40. Mathew, S. P., Gunathilagan, S., Roberts, S. M. & Blackmond, D. G. Mechanistic insights from reaction progress kinetic analysis of the polypeptide-catalyzed epoxidation of chalcone. *Org. Lett.* **7**, 4847–4850 (2005).
41. Aragonès, A. C. *et al.* Electrostatic catalysis of a Diels–Alder reaction. *Nature* **531**, 88–91 (2016).
42. Yu, M., Nowak, A. P., Deming, T. J. & Pochan, D. J. Methylated mono- and diethyleneglycol functionalized polylysines: nonionic, α -helical, water-soluble polypeptides. *J. Am. Chem. Soc.* **121**, 12210–12211 (1999).
43. Rzaev, J. Synthesis of polystyrene–polylactide bottlebrush block copolymers and their melt self-assembly into large domain nanostructures. *Macromolecules* **42**, 2135–2141 (2009).
44. Neugebauer, D., Sumerlin, B. S., Matyjaszewski, K., Goodhart, B. & Sheiko, S. S. How dense are cylindrical brushes grafted from a multifunctional macroinitiator? *Polymer* **45**, 8173–8179 (2004).

Acknowledgements

The research was supported by the US National Science Foundation (CHE-1308485 and CHE-1508710 to J.C. & DMR-1150742 to Y.L.). AFM was carried out in part in the Frederick Seitz Materials Research Laboratory Central Research Facilities, University of Illinois.

Author contributions

R.B., J.C. and Y.L. conceived the idea of the project. R.B. and Z.S. performed the experimental work. Y.L. and H.F. performed the kinetic modelling. R.B., Y.L., H.F., and J.C. wrote the manuscript with contributions from all authors. All authors discussed the results and commented on the manuscript.

Additional information

Supplementary information is available in the [online version of the paper](#). Reprints and permissions information is available online at www.nature.com/reprints. Correspondence and requests for materials should be addressed to J.C. and Y.L.

Competing financial interests

The authors declare no competing financial interests.